Energy Transfer and Thermal Accommodation in Ozone Scattering from a Perfluorinated Self-Assembled Monolayer

ARTICLE *in* THE JOURNAL OF PHYSICAL CHEMISTRY C · NOVEMBER 2012

Impact Factor: 4.77 · DOI: 10.1021/jp309733w

3 AUTHORS:

Manuel Monge-Palacios
University of Missouri
21 PUBLICATIONS **72** CITATIONS
SEE PROFILE

Juan J. Nogueira
University of Vienna
15 PUBLICATIONS **81** CITATIONS
SEE PROFILE

Emilio Martinez-Nuñez
University of Santiago de Compostela
86 PUBLICATIONS **1,021** CITATIONS
SEE PROFILE

THE JOURNAL OF PHYSICAL CHEMISTRY C

Article

pubs.acs.org/JPCC

Energy Transfer and Thermal Accommodation in Ozone Scattering from a Perfluorinated Self-Assembled Monolayer

Manuel Monge-Palacios, Juan J. Nogueira, and Emilio Martínez-Núñez*

Departamento de Química Física and Centro Singular de Investigación en Química Biológica y Materiales Moleculares, Campus Vida, Universidad de Santiago de Compostela, 15782 Santiago de Compostela, Spain

Supporting Information

ABSTRACT: A modification of the energy transfer model recently proposed by two of us (ref 4) is tested in this work by an extensive comparison with the simulation results for O_3 scattering from a perfluorinated self-assembled monolayer (F-SAM) as well as with previous NO + FSAM and Ar + F-SAM scattering results. The model fits very well the trajectory data over a $\sim 10^3$-fold of incident energies. The percentage of energy transferred to the surface, predicted by the model at high incident energies, decreases with the number of degrees of freedom of the projectile because they compete with the surface degrees of freedom as possible destinations of the incident energy. The distributions of the scattered ozone molecules over translational and rotational states show a low-energy component characterized by a Maxwell−Boltzmann (MB) distribution at the surface temperature that survives at the highest collision energies. The dependence of the fraction of the MB component on the incident energy is an exponential decay function and the rate of decay is similar for the rotational and translational distributions. A non-negligible number of the O_3 + F-SAM trajectories that penetrate the surface at high energies have very long residence times (longer than the simulation time), which enables thermal accommodation of the rotational and translational degrees of freedom. A new method to categorize the O_3 + F-SAM trajectories, based on the residence time, shows that, at very low incident energies (<10 kcal/mol), thermal accommodation can be achieved in a single collision event.

$$\langle \Delta E \rangle = a_0 + a_1 \exp(-b_1/\sqrt{E_i}) + a_2 \mathrm{csch}^2\left(\frac{b_2}{\sqrt{E_i}}\right)$$

I. INTRODUCTION

Over the last two decades, a number of experimental and theoretical studies have been devoted to understand the energy transfer dynamics in collisions of gas-phase species with organic surfaces.[1−47] The development of energy transfer models is of great interest and may facilitate the interpretation of experimental and simulation data. Those models should provide the amounts of energy transferred to the various degrees of freedom when a gas (or projectile) collides with a surface with incident energy E_i

$$E_i = \Delta E_{surf} + \Delta E_{int} + E_f \quad (1)$$

where E_f is the translational energy of the projectile after the collision, Δ indicates an energy change during the collision, E_{surf} is the surface energy, and E_{int} is the internal energy of the projectile. Previous gas-surface simulation studies show that the percentage of incident energy E_i transferred to the projectile's internal degrees of freedom $\langle \Delta E_{int} \rangle / E_i$ does not depend much on the incident energy for high values of E_i.[8,32,48,49] A model proposed previously[8] shows that the function $\exp(-b/E_i)$ (where b is a parameter) fits reasonably well the average percentage of energy transfer to the surface. This model predicts that the high E_i limiting energy transfer to the surface is ~90% for two protonated peptides scattering off a perfluorinated self-assembled monolayer (F-SAM).[8] The same model was employed by Morris and co-workers to obtain values for the high E_i limiting energy transfer to the surface of 89−98% for Ar and CO_2 scattering off several SAM surfaces.[35]

More recently, a model based on the adiabaticity parameter[50] was proposed in our group to predict the dependence of each term on the right-hand side of eq 1 on E_i.[4] This adiabatic model (AM) fits NO + F-SAM simulation results with increased accuracy compared with other models of energy transfer.[4] However, since the AM is only reliable in the adiabatic limit,[50] a modification is proposed in the present work to extend its applicability to high incident energies. The new model will be fit to the O_3 + F-SAM energy transfer results of the present work as well as to previous NO + F-SAM[4] and Ar + F-SAM[9] simulation results over a wide range of incident energies.

The amount of energy transferred to each of the degrees of freedom of eq 1 depends on the incident energy and on the collision mechanism. The trajectories are usually classified as trapping-desorption (TD) or impulsive scattering (IS), depending on the degree of thermal accommodation of the projectile. For instance a TD trajectory would lead to complete accommodation of the translational energy and the average value of E_f would be $2RT_S$ with T_S being the surface temperature. The relative fraction of TD and IS trajectories is usually determined from the distributions of the scattered molecules over their rotational $P(J)$ and translational states $P(E_f)$. In previous work[10,13,36,51,52] one or several Maxwell−Boltzmann (MB) distributions of states were employed to fit the $P(J)$ or $P(E_f)$ distributions of the scattering molecules. The

Received: October 1, 2012
Revised: November 5, 2012
Published: November 8, 2012

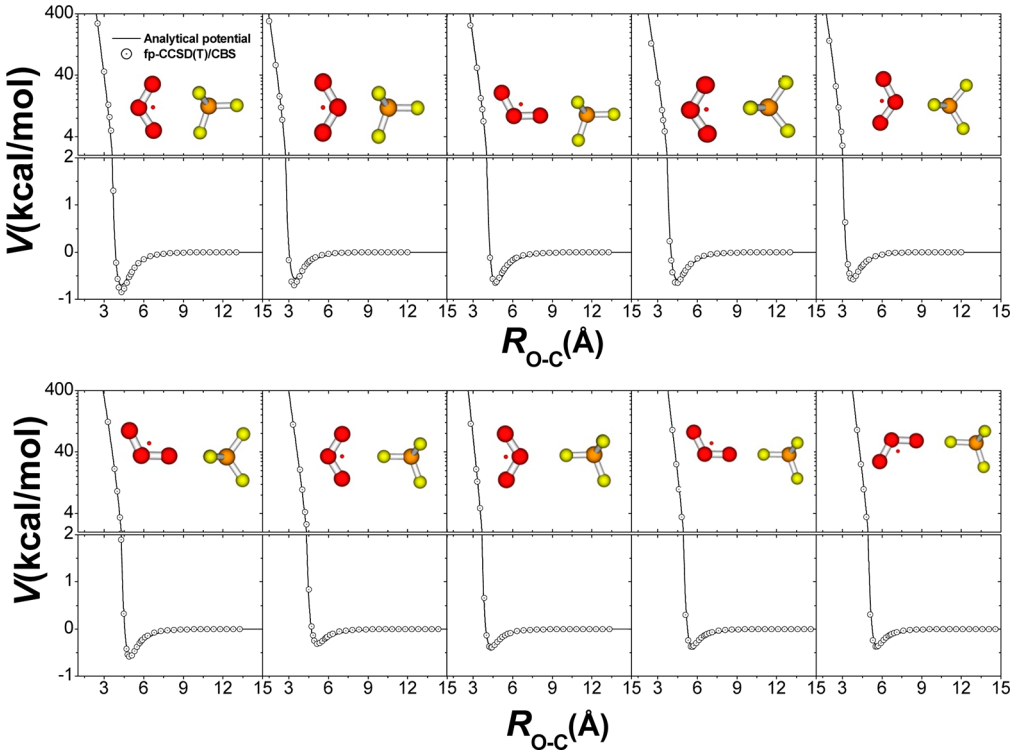

Figure 1. Analytical potential of eq 5 (solid lines) fitted to the fp-CCSD(T)/CBS ab initio calculations (circles) for different orientations of the O_3 + CF_4 system considered in this study to develop the O_3 + F-SAM interaction potential. The small red dot in the middle of the terminal oxygen atoms represents the pseudoatom that has been considered as an additional interaction site to improve the fit (see text).

simplest interpretation of the experimental or simulation results is that the distribution of the TD trajectories resembles a MB distribution at the surface temperature T_S, whereas that of the IS trajectories corresponds to a temperature that is well above T_S. This means that, if the total $P(J)$ or $P(E_f)$ distribution has two components, the low-energy component would correspond to TD and the high-energy component to IS.

However, chemical dynamics simulations of gas-phase species scattering off SAMs indicate that the collision process may be considerably more complex than the above TD/IS model. For instance, it was found that direct events, without trapping on the surface, may contribute to the low-energy component of the distribution, and, on the other hand, trajectories that physisorb or penetrate inside the monolayers may contribute to the high-energy component of the distribution.[6,10,18,21,53] In particular, recent CO_2 + F-SAM scattering calculations show that TD cannot be unambiguously identified with the low-energy component of the $P(E_f)$ distribution.[6] It is therefore of great interest to classify the trajectories in a way that can help interpret the rotational and translational distributions of the scattering gases. In the present article, the O_3 + F-SAM trajectories are sorted according to their residence time, that is those with short residence times will contribute to the high-energy portion of the distribution, whereas those with long residence times will lead to thermal accommodation and they will be part of the low-energy component.

II. COMPUTATIONAL DETAILS

A. Potential Energy Surface. The potential energy function of the O_3 + F-SAM system reads:

$$V = V_{surf} + V_{O_3} + V_{O_3-surf} \quad (2)$$

The first term V_{surf} describes the interactions that take place in the F-SAM surface,[9,10] V_{O_3} is the ozone potential function, and V_{O_3-surf} accounts for the interaction between ozone and the surface.

The F-SAM surface consists of 48 chains of $CF_3(CF_2)_7S$ radicals adsorbed on a single layer of 225 Au atoms, which are kept fixed during the dynamics simulations; all atoms are explicitly considered in our model. A molecular dynamics simulation of the monolayer provides a 300 K structure of the surface in close agreement with experiment, that is the monolayer forms a hexagonal close-packed structure with the nearest-neighbor direction rotated 30° with respect to the Au{111} lattice and the backbone of the $CF_3(CF_2)_7S$ moiety has a tilt angle with respect to the surface normal of ∼12°.[10]

The ozone intramolecular potential function V_{O_3} is harmonic:

$$V_{O_3} = \sum \frac{1}{2}k_r(r_{OO} - r_{OO}^{eq})^2 + \frac{1}{2}k_\theta(\theta - \theta^{eq})^2 \quad (3)$$

where the force constants k_r and k_θ are adjusted to fit the ab initio vibrational frequencies of ozone calculated in this work at the CCSD(T)(full)/aug-cc-pVQZ level of theory. The ab initio frequencies 728 (A_1), 1174 (A_1), and 1087 (B_2) cm^{-1} compare well with those predicted by eq 3: 642 (A_1), 1051 (A_1), and 1107 (B_2). The resulting values of the force constants are: k_r = 4.7 mdyn × $Å^{-1}$ and k_θ = 2.3 mdyn × Å/rad^2. The O−O equilibrium distance r_{OO}^{eq} and the equilibrium angle θ^{eq} are taken from the CCSD(T)(full)/aug-cc-pVQZ calculation and are 1.266 Å and 117.3°, respectively.

The O_3/F-SAM interaction potential V_{O_3-surf} was obtained from high-level ab initio data for the O_3 + CF_4 system.[3,9,10,54−56] This means that the carbon and fluorine atoms in CF_4 are considered equivalent to those in F-SAM.

dx.doi.org/10.1021/jp309733w | J. Phys. Chem. C 2012, 116, 25454−25464

Table 1. Parameters of the O_3−CF_4 Intermolecular Analytical Potential of Eq 5[a]

$i-j$[b]	A_{ij}	B_{ij}	C_{ij}	D_{ij}	E_{ij}	F_{ij}
O_1−C	1494.696	2.485				
O_2−C	77000.000	4.491	1343.061	6.963	10.784	16.000
X−C	200000.000	4.702	−109.759	4.339	274.976	19.581
O_1−F	177000.000	4.606	−376.281	6.505	24.400	20.761
O_2−F	34425.742	3.837	−236.131	5.311	368.188	9.443
X−F	7.386	7.947	115.532	4.783		

[a]Units are such that potential energy is in kcal/mol and distance is in Å. [b]O_1, O_2, and X refer to the central and terminal oxygen atoms and to the pseudo atom, respectively.

This approach provides gas-surface interaction energies that agree very well with those obtained using more realistic models for the F-SAM surface.[3]

MP2(FC)/aug-cc-pVXZ (X = D,T,Q) and CCSD(T)(FC)/aug-cc-pVDZ single point energies were computed for the relative orientations of O_3 and CF_4 shown in Figure 1. The ab initio calculations, carried out with *Gaussian09*,[57] include the counterpoise correction to account for the basis set superposition error (BSSE).[58] The MP2(FC)/aug-cc-pVXZ values were extrapolated to the complete basis set limit (CBS) using Peterson's approach:[59]

$$E(n) = E_{CBS} + A\exp[-(n+1)] + B\exp[-(n+1)^2] \quad (4)$$

with n = 2, 3, 4 for X = D, T, Q respectively and $E(n)$ being the MP2(FC)/aug-cc-pVXZ energy. To obtain more accurate energies, the focal-point approximation of Allen and coworkers[60] has been employed in this study. The method takes advantage of the fact that, usually, for large basis sets, the difference between the MP2 and CCSD(T) energies is independent of the basis set. In this work, CCSD(T) energies at the CBS limit (here and after fp-CCSD(T)/CBS) were computed with the focal point approach.

The analytical function employed to fit the fp-CCSD(T)/CBS interaction energies is a sum of two-body Buckingham potentials:

$$V_{O_3-surf} = \sum_{ij} A_{ij}\exp(-B_{ij}R_{ij}) + C_{ij}/R_{ij}^{D_{ij}} + E_{ij}/R_{ij}^{F_{ij}} \quad (5)$$

where i and j represent each of the atoms of the O_3 and CF_4 molecules respectively R_{ij} is the i−j interatomic distance and A_{ij}, B_{ij}...F_{ij} are the parameters. For ozone we added a pseudoatom in the middle of the two terminal oxygen atoms to improve the fit, which was conducted using a genetic algorithm.[61] To avoid the Buckingham catastrophe some restrictions were imposed to the parameters, namely, all D_{ij} parameters range from 4 to 7, all E_{ij} parameters are positive and all F_{ij} parameters are greater than 9.

Figure 1 shows the resulting interaction potential (solid line) and the final two-body parameters are collected in Table 1. The stratified root-mean-square error of the fit is 5×10^{-2} kcal/mol for energies lower than 2 kcal/mol and 6.8 kcal/mol for energies in the range 2−400 kcal/mol.

Finally, to prevent ozone from unphysical penetration through the gold slab, an O−Au potential function was added. In the absence of accurate potential functions for O interacting with gold the repulsive part of the O−C two-body potential was employed.[10,62] An additional drawback of our potential function is the lack of an O−S interaction potential. However, overall, the strategy employed to construct the model potential function seems to be pretty accurate and simulation results obtained with this model agree very well with experiment (see below for O_3 + F-SAM and also see refs 4,6,9,10 for other systems).

B. Chemical Dynamics Simulations. Batches of 2000 trajectories were run for the following incident energies in kcal/mol: 1, 5, 10, 16.75, 50, 100, 200, and 400. The energy of 16.75 kcal/mol corresponds to the experiment carried out by Morris and co-workers.[63] Each vibrational mode of ozone has the zero-point vibrational energy and the initial rotational energy about each rotational axis was $1/2k_BT_{rot}$ with T_{rot} = 20 K. The projectiles were collided perpendicularly (θ_i = 0°) with the surface. For the incident energy of 16.75 kcal/mol, an additional batch of 10 000 trajectories was run with an incident angle of θ_i = 30° and T_{rot} = 298 K, to mimic the experimental conditions of Morris and co-workers;[63] in this case, the azimuthal angle χ, defined as the projection of the velocity vector onto the surface plane, was randomly selected between 0 and 2π.

All of the simulations were carried out using the *VENUS05* computer program.[64,65] The trajectories were integrated with a fixed step size of 0.3 fs using the Adams-Moulton algorithm for a total integration time of 60 ps. Before the beginning of each trajectory simulation, the surface was relaxed to a thermodynamic equilibrium structure by a 2 ps molecular dynamics simulation[66] in which the atomic velocities are scaled to obtain a surface temperature of 300 K. This structure was then used as the initial structure of a 100 fs equilibration run at the beginning of each trajectory. Periodic boundary conditions were also utilized to simulate a larger surface.[66] After the integration of each trajectory, the surface energy and the translational and internal energies of the scattered ozone molecules were calculated from the atomic Cartesian coordinates and momenta.

III. RESULTS AND DISCUSSION

A. Reliability of the Simulation Results and Comparison with Experiment. An stringent test of the methodology employed in this work consists of comparisons of the simulation results with experiment. Morris and co-workers[63] carried out molecular beam experiments of ozone scattering from a perfluoro alkanethiol SAM on gold. They measured the $P(E_f)$ distributions for an incident energy of 16.75 kcal/mol and incident angle with respect to the surface normal θ_i of 30°. The final E_f values were obtained for the gases that scattered specularly from the F-SAM, that is, for final scattering angles of 30°. Figure 2 compares the experimental $P(E_f)$ distribution (solid circles) with our simulation results (histogram). The simulation $P(E_f)$ distribution is obtained for the whole scattering flux since our results show that the distribution is unaffected, within statistical errors, by the final scattering angle. Troya et al. also found that the $P(E_f)$ distributions obtained in

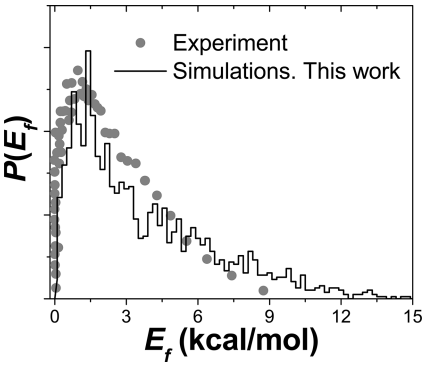

Figure 2. $P(E_f)$ distribution obtained in our simulation study (histogram) compared with the experimental results (circles) at E_i = 16.75 kcal/mol and θ_i = 30°.

their classical trajectory study of collisions of HCl with hydroxylated alkanethiol self-assembled monolayers are essentially independent of the recoil angle.[67] Although the simulation $P(E_f)$ distribution is slightly hotter than the experimental one, both peak at a value of E_f ~1.5 kcal/mol. Additionally, Morris and co-workers[63] found that ~40% of the $P(E_f)$ distribution corresponds to a MB component at the surface temperature compared with the 38% obtained in this work. The comparison of our simulation results with experimental data suggests that our simulation results are reliable.

Because the simulations are carried out at very high incident energies (the highest being 400 kcal/mol), some comments about the accuracy of the ozone potential function should be added at this point. The potential energy surface of ozone presents a conical intersection (CI) connecting the ground state with the lowest excited state of the same symmetry ($^1A_1$).[68] The CI lies 53.6 kcal/mol above the ground state minimum and has a bond angle of 83.2°. Because the highest incident energies of our simulation study are well above 53.6 kcal/mol, it is of interest to see whether nonadiabatic effects could affect the dynamics of our system. The simulations show that, even at the highest E_i of 400 kcal/mol, the average amount of energy transferred to the ozone vibrational modes is modest and lower than 17 kcal/mol (vide infra). Moreover, the minimum bond angle of ozone attained at any point of our simulations is always greater than 85°. These findings suggest, therefore, that ozone molecules stay in their ground electronic state throughout the dynamics, even at the highest incident energies.

On the other hand, the bond dissociation energy of ozone is only ~24 kcal/mol,[68] which enables surface-induced dissociation (SID) of the molecule at high incident energies. However, SID and possible reactions between ozone and the F-SAM are not described by the model potential energy function employed in this study.

B. Energy Transfer. A model based on the adiabaticity parameter[50] was recently proposed by two of us to rationalize the extent of energy transfer between a diatomic molecule and an F-SAM.[4] Very briefly, the adiabaticity parameter is defined as[50]

$$\xi = \frac{a}{v_i t_v} \tag{6}$$

where a is the range of the intermolecular force, v_i is the relative velocity of the colliding partners (or incident velocity in our case) and t_v is the vibrational period of the diatomic molecule. The model assumes the following functional form for the average amount of energy transfer to vibration of the projectile:[4]

$$\langle \Delta E^{ad} \rangle = \langle \Delta E \rangle_{v_i \to 0} + \langle \Delta E \rangle^{sudden} \exp\left(-\frac{a}{v_i t_v}\right) \tag{7}$$

where the superscript ad (adiabatic) is used to emphasize that the applicability of the model limits to low incident energies. The term $\langle \Delta E \rangle_{v_i \to 0}$ is included in eq 7 to account for the non-negligible energy transfer in the $v_i \to 0$ limit and $\langle \Delta E \rangle^{sudden}$ is the average energy transfer in the sudden limit ($\xi = 0$). Eq 7 can be recast in the form:

$$\langle \Delta E^{ad} \rangle = a_0 + a_1 \exp(-b_1/\sqrt{E_i}) \tag{8}$$

where a_1 and b_1 are parameters that can be fit to simulation or experimental data, $E_i = 1/2 M v_i^2$, M is the mass of the projectile, and a_0 can be determined assuming complete accommodation at low incident energies, that is, $a_0 = k_B T_S$ for energy transfer to rotation of the diatomic molecule or $a_0 = 2k_B T_S$ for energy transfer to translation.

Eq 8 was successfully fit to NO + F-SAM simulation results for E_i < 40 kcal/mol,[4] but its applicability to higher incident energies is uncertain. For high incident energies we propose to employ an adaptation of the impulsive approximation of Mahan for energy transfer to a harmonic oscillator:[69]

$$\frac{\langle \Delta E^{imp} \rangle}{E_i} = C\left(\frac{\pi \omega a}{v_i}\right)^2 \mathrm{csch}^2\left(\frac{\pi \omega a}{v_i}\right) \tag{9}$$

where ω is the frequency of the harmonic oscillator and C is a constant that depends on the masses of the atoms involved in the collision. The above equation can be rewritten in the following form

$$\langle \Delta E^{imp} \rangle = a_2 \mathrm{csch}^2\left(\frac{b_2}{\sqrt{E_i}}\right) \tag{10}$$

with a_2 and b_2 being two adjustable parameters. As E_i increases, eq 10 presents a linear dependence on E_i with slope a_2/b_2^2.

The phenomenological model proposed in this work is an adaptation of the above two limiting models, originally developed for atom−diatom collisions. In our model, the diatom is replaced by a projectile (of any size) and the surface plays the role of the atom. The amount of energy transfer to each of the degrees of freedom of the projectile is thus:

$$\langle \Delta E \rangle = \langle \Delta E^{ad} \rangle + \langle \Delta E^{imp} \rangle = a_0 + a_1 \exp(-b_1/\sqrt{E_i}) + a_2 \mathrm{csch}^2\left(\frac{b_2}{\sqrt{E_i}}\right) \tag{11}$$

with a_1, b_1, a_2, and b_2 being adjustable parameters.

The model shows a linear dependence of $\langle \Delta E \rangle$ versus E_i for high incident energies, which explains the fairly constant values of $\langle \Delta E_{int} \rangle / E_i$ as a function of the incident energy found previously for a number of systems.[8,32,48,49]

Figure 3 shows the average values of energy transferred to vibration, rotation and translation of the projectile obtained in our O_3 + F-SAM simulations (symbols) and the fits of eq 11 to the simulation data (solid lines). The parameters obtained in the fits are collected in Table 2. A unitless quantity of interest is the fraction of energy $\langle \Delta E \rangle / E_i$ transferred to each of the

dx.doi.org/10.1021/jp309733w | J. Phys. Chem. C 2012, 116, 25454−25464

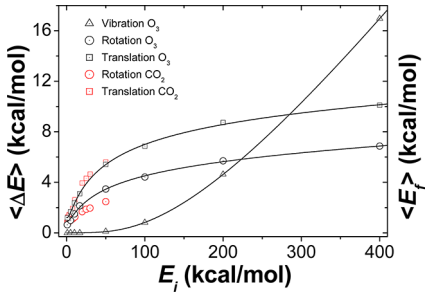

Figure 3. Amount of energy transferred to vibration (triangles), rotation (circles), and translation (squares) of ozone in the O_3 + F-SAM collision process as a function of E_i. The fit of the energy transfer model proposed in this work to the simulation data is shown as solid lines. Our previous CO_2 + F-SAM energy transfer results are also depicted for comparison.[6]

Table 2. Parameters of the Energy Transfer Model for O_3 + F-SAM

parameter[a]	vibration	rotation	translation
a_1	0.16	7.45	11.9
a_2	74.9	0.055	0.0059
b_1	12.1	7.88	7.53
b_2	29.8	4.75	1.75

[a]The units are such that $\langle\Delta E\rangle$ is in kcal/mol. The values of a_0 are 0.0, 0.9 ($3/2k_BT_S$) and 1.2 ($2k_BT_S$) kcal/mol for vibration, rotation, and translation, respectively.

degrees of freedom; this fraction is called here energy transfer efficiency (ETE). In the limit of infinite incident energy ETE(∞) to the degrees of freedom of the molecule is obtained from the model parameters as a_2/b_2^2 and ETE(∞) to the surface can be obtained from energy conservation (eq 1). The values of ETE(∞) to the vibrational, rotational and translational degrees of freedom of ozone are (in percentage) 8.4, 0.2 and 0.2, respectively. Figure 4 shows the results for ETE to the

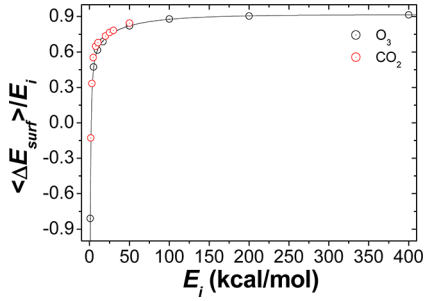

Figure 4. ETE to the surface ($\langle\Delta E_{surf}\rangle/E_i$) as a function of E_i obtained in this work for O_3 + F-SAM. The prediction of the energy transfer model proposed in this work is shown as a solid line. Our previous CO_2 + F-SAM energy transfer results are also depicted for comparison.[6]

surface, with the model results (solid line) being obtained from the previous fits (Table 2) and conservation of energy (eq 1). The value of ETE(∞) to the surface obtained according to our model is 91.2%. Also shown in Figures 3 and 4 are previous CO_2 + F-SAM simulation results, which closely follow the present O_3 + F-SAM results.[6]

As a further test of the model, eq 11 was fit to NO + F-SAM[4] and Ar + F-SAM[9] simulation results. For NO + F-SAM, new simulations are carried out here for E_i = 100, 250, and 500 kcal/mol. At these high incident energies, a new potential for the interaction between NO and the surface was employed (Supporting Information). Figure 5 and Table 3 show the

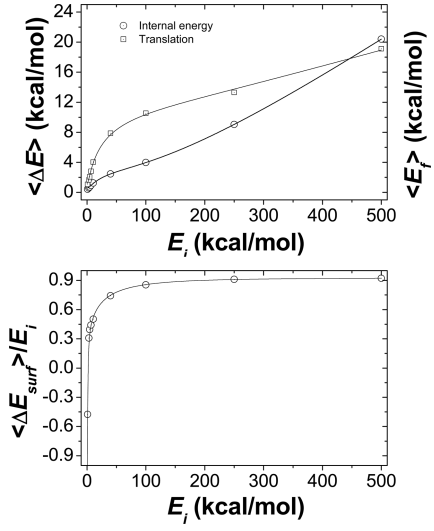

Figure 5. Amount of energy transferred to the internal states (circles), and translation (squares) of nitric oxide in the NO + F-SAM collision process as a function of E_i (upper plot) and ETE to the surface as a function of E_i (lower plot). The fit of the energy transfer model proposed in this work to the simulation data is shown as solid lines. Some data are taken from our previous work.[4].

Table 3. Parameters of the Energy Transfer Model for NO and Ar + F-SAM

	NO + F-SAM		Ar + F-SAM
parameter[a]	internal	translation	translation
a_1	6.20	16.2	11.6
a_2	47.9	30.2	17.9
b_1	7.70	5.82	4.77
b_2	29.8	36.0	31.8

[a]The units are such that $\langle\Delta E\rangle$ is in kcal/mol. The values of a_0 are 0.9 (k_BT_S) and 1.2 ($2k_BT_S$) kcal/mol for the internal energy and translation, respectively.

resulting fits to the NO + F-SAM energy transfer data. The values of ETE(∞) to the internal and translational degrees of freedom of the projectile are 5.4% and 2.3%, respectively; ETE(∞) to the surface is 92.3%, a value slightly higher than that found for ozone.

Our previous Ar + F-SAM simulations are extended in this work to incident energies up to 1500 kcal/mol, using the original model parameters.[9] Figure 6 and Table 3 show the fits of our model to the Ar + F-SAM results. In the limit of high incident energies, 1.8% of the incident energy goes to translation and the remaining 98.2% goes to the surface. The value of ETE(∞) to the surface is substantially higher than that obtained for NO and O_3. Experimental studies on rare gases scattering off gold and platinum surfaces[70] show that the values of ETE(∞) to the surface are also very close to 100%.

Table 4 collects a summary of ETE(∞) to the various degrees of freedom. Previous results from Hase's group for two big projectiles (Ala_2-H^+ and Gly_2-H^+) colliding with the same F-SAM are included for comparison; the values of ETE(∞) for Ala_2-H^+ and Gly_2-H^+ + F-SAM are obtained from the simulation results at E_i = 70 eV.[8] As seen in the table,

dx.doi.org/10.1021/jp309733w | J. Phys. Chem. C 2012, 116, 25454−25464

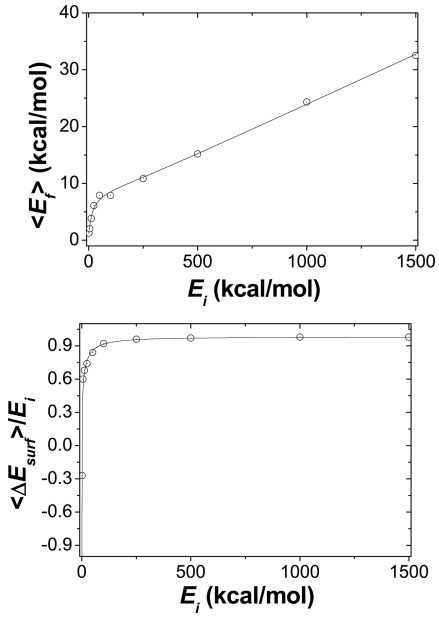

Figure 6. Amount of energy transferred to translation (symbols) of Ar in the Ar + F-SAM collision process as a function of E_i (upper plot) and ETE to the surface as a function of E_i (lower plot). The fit of the energy transfer model proposed in this work to the simulation data is shown as solid lines. Some data are taken from our previous work.[9]

Table 4. ETE(∞) (in %) to the Various Degrees of Freedom for Several Projectiles[a]

	Ar	NO	O_3	Gly_2-H^+	Ala_2-H^+
translation	1.8	2.3	0.2	4	4
internal	0.0	5.4	8.6	13	13
surface	98.2	92.3	91.2	83	83

[a]In all cases the projectiles collide with an F-SAM. The results for Gly_2-H^+ and Ala_2-H^+ are taken from ref 8 and refer to perpendicular collisions at E_i = 70 eV.

ETE(∞) to the internal degrees of freedom of the projectile increases with the number of degrees of freedom (n_{dof}), with a concomitant decrease of ETE(∞) to the surface. Figure 7 shows the dependence of ETE(∞) to the internal states of the molecule $ETE^{int}(\infty)$ with n_{dof} of each projectile. The values of $ETE^{int}(\infty)$ seem to plateau for a sufficiently high value of n_{dof} and the following equation was fit to the simulation results:

$$ETE^{int}(\infty) = A\exp(-B/n_{dof}) \quad (12)$$

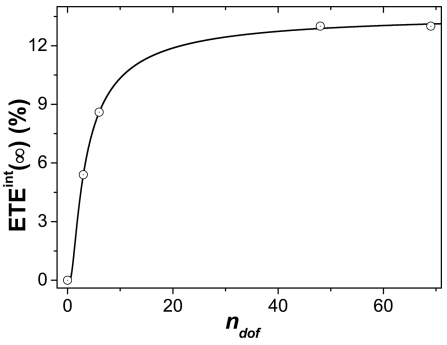

Figure 7. ETE to the surface (expressed as percentage) as a function of n_{dof} for several projectiles (text) colliding with the same F-SAM.

The resulting parameters are A = 13.6% and B = 2.8 degrees of freedom. Work is in progress in our group to see whether the asymptotic behavior of $ETE^{int}(\infty)$ observed for the 5 gases of this work explains the results for other systems. Scattering calculations are currently underway for different projectiles of increasing complexity colliding with an F-SAM.

The model proposed here entails an improvement over the one proposed recently to explain the NO + F-SAM simulations.[4] Although it has been tested with energy transfer data for collisions of gases with organic surfaces, it should be valid also for other types of surfaces. A limitation of the model is the neglect of reactive scattering.

C. Collision Types. To compare the present O_3 + F-SAM simulation results with previous work done in our group, the trajectories are labeled according to both the minimum height of the projectile center-of-mass above the gold surface h_{min} and to the number of inner turning points in the direction perpendicular to the surface ITPs.[4] For a penetrating trajectory h_{min} < 11.6 Å (see ref 4 for the details). The remaining collisions are either called direct, when ITPs = 1, or physisorption, if ITPs > 1.

The percentages of the different trajectory types found in our O_3 + F-SAM study are plotted in Figure 8 (upper plots) as a

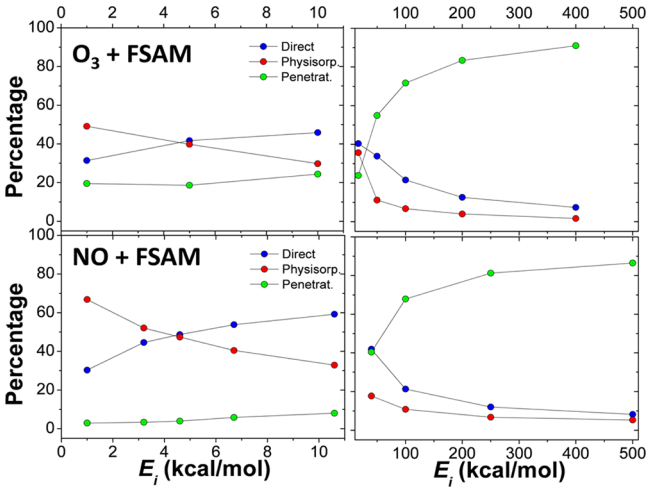

Figure 8. Percentages of the different collision events (text) as a function of the incident energy E_i obtained in our O_3 + F-SAM study (upper plots). The lower plots show the corresponding percentages for the NO + F-SAM system.

function of E_i. For comparison purposes, the figure also collects the previous results for NO + F-SAM[4] complemented with additional calculations for high incident energies (lower plots). Quite interestingly, there seems to be two distinct behaviors as a function of the incident energy for both systems. At low incident energies (E_i < 50 kcal/mol), direct collisions increase with E_i with a concomitant decrease of physisorption; penetration remains fairly constant in this range of incident energies. Quite remarkably the crossover between the amount of direct collisions and physisorption occurs at ∼5 kcal/mol for both O_3 and NO + F-SAM.

At high incident energies, though, direct collisions decrease with E_i at the expense of penetration. Figure 9 shows that, at the highest E_i (close to 400 kcal/mol), most of the O_3 + F-SAM trajectories penetrate the monolayer directly (direct−penetration), and only 1% of the molecules interact with the terminal CF_3 groups before penetration, which is called here

dx.doi.org/10.1021/jp309733w | J. Phys. Chem. C 2012, 116, 25454−25464

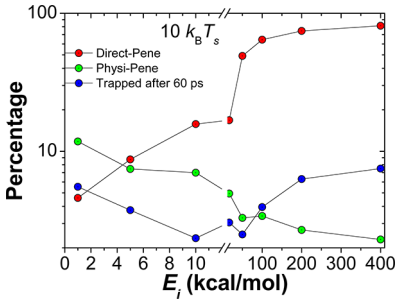

Figure 9. Percentages of the different penetration mechanisms found in our O_3 + F-SAM study (text) as a function of the incident energy E_i.

physisorption−penetration. Additionally, 8% of the molecules remain trapped inside the monolayer for a long time (>60 ps) at E_i = 400 kcal/mol. The importance of penetration and trapping in gas/surface scattering has been highlighted in previous work. Troya and co-workers found that surface penetration is important for Ar + F-SAM when Ar collides with a small incident angle with respect to the surface normal at E_i = 6−12 eV.[71] Sibener and co-workers pointed out a new mechanism for the incorporation of gaseous moieties in the surface region of ice by which Xe atoms are embedded in amorphous and crystalline ice at hyperthermal incident energies.[72] Similarly, Cooks and co-workers proposed a method to prepare modified surfaces, referred to as soft-landing, where intact polyatomic ions are deposited from the gas phase into a F-SAM at E_i = 10 eV.[73] Preliminary simulation results in our group show that indeed when $SiNCS^+$ and $(CH_3)_2SiNCS^+$ collide perpendicularly with an F-SAM at E_i = 10 eV the vast majority of the trajectories (~90%) remain trapped inside the monolayer for more than 60 ps.

D. Accommodation of the Rotational and Translational Degrees of Freedom of the Projectile. As indicated in the introduction, there is compelling evidence that trajectories of the same type (according to the above classification, i.e., direct, physisorption, and penetration) may lead to different degrees of thermal accommodation of the molecule's degrees of freedom.[6,10,18,21,53] Accommodation of the degrees of freedom of the projectile at the surface can be quantified by using an accommodation coefficient. Knudsen, based on Maxwell's seminal work on collisions of gases with walls, defined the accommodation coefficient as[74−76]

$$\alpha = \frac{E_i - \langle E_f \rangle}{E_i - 2k_B T_S} \tag{13}$$

where $\langle E_f \rangle$ is the average translational energy of the projectile following scattering at the surface. Analogously, the portion of the $P(E_f)$ distribution at the surface temperature (the low-energy component), which will be called here β, is also a good metric for accommodation. As shown below, α and β are not necessarily equal and they provide the same value when the high-energy component of $P(E_f)$ arises exclusively from elastic collisions, or for complete accommodation ($\langle E_f \rangle = 2k_B T_S$ and $\alpha = \beta = 1$). Assuming the $P(E_f)$ distribution is written as a weighted sum of a MB component at T_s $P^{MB}_{T_s}(E_f)$ and a high-energy component $P^{HE}(E_f)$

$$P(E_f) = \beta P^{MB}_{T_S}(E_f) + (1 - \beta) P^{HE}(E_f) \tag{14}$$

then, the average value of E_f is

$$E_f = \beta 2k_B T_S + (1 - \beta)\langle P^{HE}\langle E_f \rangle\rangle \tag{15}$$

which can be inserted in eq 13 to give

$$\alpha(E_i - 2k_B T_S) = \beta(\langle P^{HE}(E_f)\rangle - 2k_B T_S) + E_i - \langle P^{HE}(E_f)\rangle \tag{16}$$

From eq 16, it is clear that if the high-energy component of $P(E_f)$ is associated to a mechanism of elastic collisions (i.e., $P^{HE}(E_f) = E_i$), then $\alpha = \beta$. However, SAM surfaces absorb an important fraction of the incident energy and therefore, for these surfaces, α differs from β. In this work, the coefficient β is termed accommodation coefficient and it will determined from the $P(E_f)$ and $P(J)$ distributions using two different methods as indicated below.

In the fitting method, a MB distribution at T_S will be fit to a portion (the low-energy portion) of the simulation $P(E_f)$ and $P(J)$ curves; this portion of the distribution is β. This method has been employed in previous work.[10] The corresponding MB distributions of translational and rotational states of ozone following scattering at the F-SAM are:

$$P^{MB}_{T_S}(E_f) = (k_B T_S)^{-2} E_f \exp(-E_f/k_B T_S) \tag{17}$$

$$P^{MB}_{T_S}(J) = N(2J+1)\exp\left(-\frac{B' hcJ(J+1)}{k_B T_S}\right) \sum_{K=-J}^{J} \exp\left(-\frac{hc(A - B')K^2}{k_B T_S}\right) \tag{18}$$

eq 18 assumes that ozone is a prolate top and the rotational constant $B' = (BC)^{1/2}$. This assumption is supported by the fact that the asymmetry parameter κ is −0.97. The rotational constants of ozone are calculated from the parameters of our potential function (r^{eq}_{OO} and θ^{eq}) and are: A = 3.64253 cm^{-1}, B = 0.45120 cm^{-1}, and C = 0.40147 cm^{-1}. Figure 10 shows an

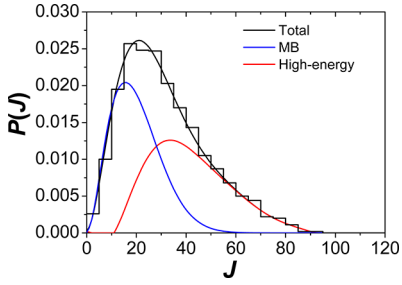

Figure 10. $P(J)$ distribution obtained in our simulations (black line) for E_i = 16.75 kcal/mol. The blue and red lines are the corresponding MB and high-energy distributions. The area under the MB distribution at T_S is β (0.5 in this case).

example of how β is obtained in the fitting method for the $P(J)$ distribution at E_i = 16.75 kcal/mol. The blue line is the MB distribution at T_S and the area under this curve is β, which in this case is 0.5.

The second method, termed here overlap method, is based on recent work done in our group on NO + F-SAM.[4] This previous study revealed that, rather than sorting the trajectories according to the ITPs, thermal accommodation can be more easily understood by looking at the residence time.[4] In the overlap method, a new classification of the trajectories, based on the residence time τ_{res}, is proposed. There are two types of

dx.doi.org/10.1021/jp309733w | J. Phys. Chem. C 2012, 116, 25454−25464

trajectories: (a) those with long τ_{res} (that will reach thermal equilibrium) and (b) those with short τ_{res} (that will not achieve thermal equilibrium). In practice, several $P(E_f)$ and $P(J)$ curves are obtained for trajectories with values of τ_{res} greater than a given value τ_{res}^0. Figure 11 shows the trajectory distributions

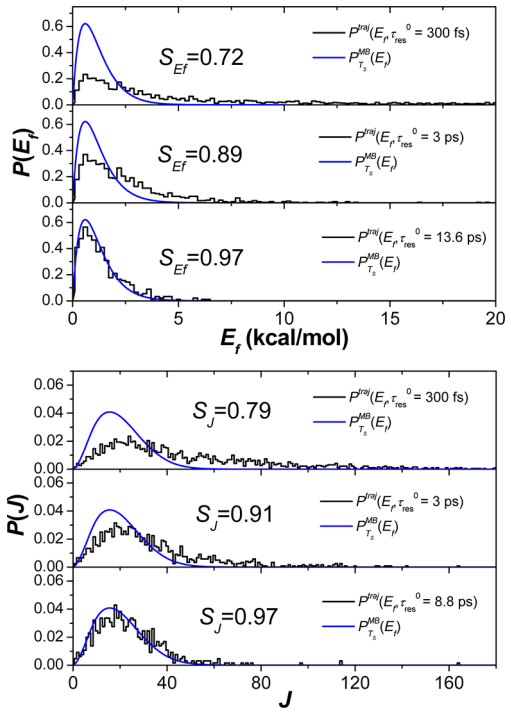

Figure 11. $P(E_f)$ and $P(J)$ distributions obtained in our simulations (histograms) obtained for different residence times (text) for E_i = 400 kcal/mol, in comparison with the corresponding MB distributions at the surface temperature (solid blue lines). The values of the overlaps of both distributions are indicated in the plots.

(P^{traj}, histograms) and the MB distribution at T_S (P_{TS}^{MB}, blue line) for the simulation at E_i = 400 kcal/mol; quite clearly, as τ_{res}^0 increases, P^{traj} approaches P_{TS}^{MB}. A measure of the resemblance of the P^{traj} and P_{TS}^{MB} distributions is the overlap S of both. Two overlaps are calculated here S_{E_f} and S_J, for the translational and rotational distributions, respectively:

$$S_{E_f}(\tau_{res}^0) = \int_{\infty}^{0} [P^{traj}(E_f, \tau_{res}^0) P_{T_S}^{MB}(E_f)]^{1/2} dE_f \quad (19)$$

$$S_J(\tau_{res}^0) = \sum_{\infty}^{J=0} [P^{traj}(J, \tau_{res}^0) P_{T_S}^{MB}(J)]^{1/2} \quad (20)$$

The residence time τ_{res} is defined as the time spent by the molecule at a height of 25 Å or less above the gold surface. At this height the force and torque exerted on the molecule are negligible. Figure 12 shows that both S_{E_f} and S_J reach a plateau close to unity for values of τ_{res}^0 around 9−14 ps for the simulation at E_i = 400 kcal/mol. This time span corresponds to the onset of accommodation, that is, this is the minimum residence time that the molecules need to come to thermal equilibrium with the surface (this residence time is called here $\tau_{res}^{0,acc}$). The smooth leveling off of the overlap curves precludes an accurate determination of $\tau_{res}^{0,acc}$. The practical way followed here to qualitatively determine $\tau_{res}^{0,acc}$ is to calculate an average value (for 5 ps) of S around its maximum, then $\tau_{res}^{0,acc}$ is

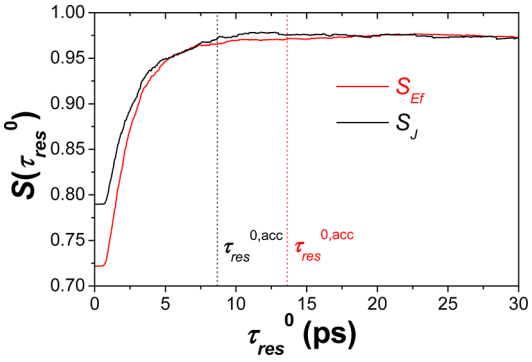

Figure 12. Overlap of the rotational S_J (black) and translational distributions S_{E_f} (red) as a function of τ_{res}^0 (text) for E_i = 400 kcal/mol.

defined as the minimum value of τ_{res}^0 for which the overlap equals its average value around the maximum.

According to the overlap method presented above, the accommodation coefficient β is given by the fraction of trajectories with $\tau_{res} > \tau_{res}^{0,acc}$. Figure 13 shows an example of

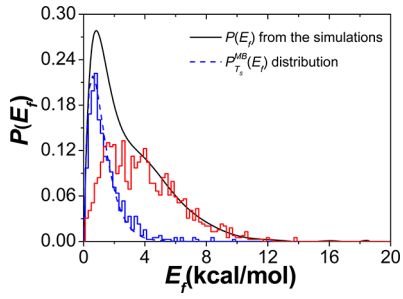

Figure 13. $P(E_f)$ distributions obtained in our simulations for E_i = 16.75 kcal/mol and θ_i = 0°. At this incident energy the value of $\tau_{res}^{0,acc}$ is 7 ps. The results for all trajectories are shown as a black line, those trajectories with $\tau_{res} > \tau_{res}^{0,acc}$ are depicted as a blue histogram, and those trajectories with $\tau_{res} < \tau_{res}^{0,acc}$ as a red histogram; the MB distribution at T_S is shown as a dashed blue line.

the $P(E_f)$ distribution obtained in our simulations for E_i = 16.75 kcal/mol. The blue histogram is the distribution obtained for those trajectories with $\tau_{res} > \tau_{res}^{0,acc}$ = 7 ps and the MB distribution at T_S is indicated as a dashed blue line; the red histogram is the distribution for those trajectories with $\tau_{res} < \tau_{res}^{0,acc}$ = 7 ps.

Figure 14 shows the dependence of β on E_i obtained in this work with the fitting and overlap methods. The figure shows that both methods predict, at least qualitatively, similar values of β, that is the accommodation coefficients decrease markedly for the lowest incident energies and then, for higher incident energies, they plateau around 0.3−0.4. The dependence of β on E_i follows reasonably well an exponential decay

$$\beta = a + (1 - a)\exp(-bE_i) \quad (21)$$

where the parameters a and b are determined by fitting eq 21 to the average values of β obtained by the fitting and overlap methods (the fit is shown in Figure 14). The value of b obtained for the translational and rotational degrees of freedom is similar and around 0.10 mol/kcal, which suggests that the accommodation process is similar for both degrees of freedom. The dependence of β on E_i found in this work is at variance with the general assumption that this coefficient should

dx.doi.org/10.1021/jp309733w | J. Phys. Chem. C 2012, 116, 25454−25464

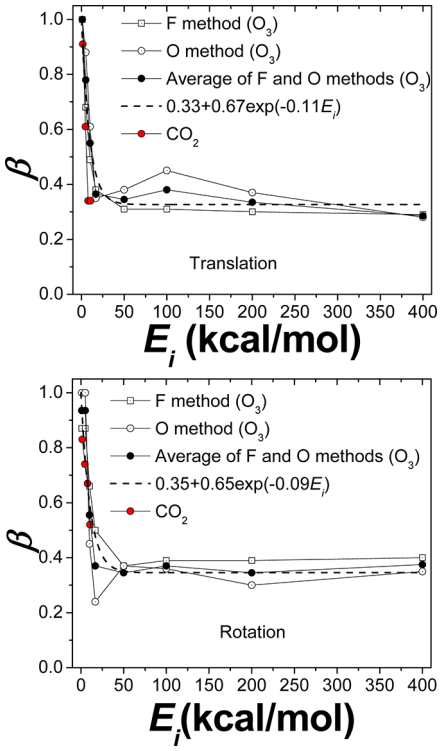

Figure 14. Accommodation coefficients β obtained by the fitting (F) and overlap (O) methods, the average of both coefficients and an exponential decay function that fits the average values. Our previous results for CO_2 + F-SAM are also depicted for comparison.[6].

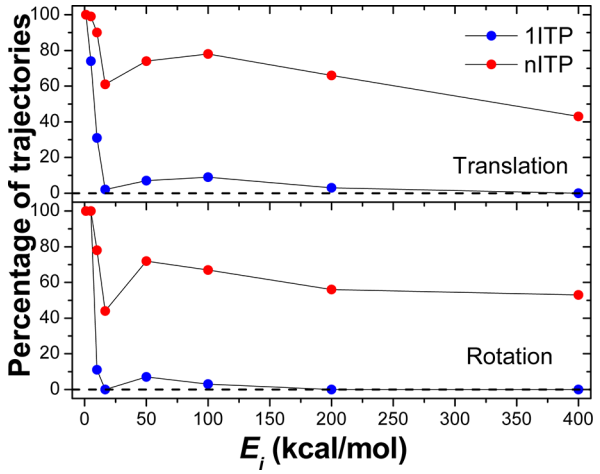

Figure 15. Percentages of trajectories that perform one (blue) or multiple (red) collisions and achieve accommodation of the translational and rotational degrees of freedom of ozone, according to the overlap method.

approach zero as E_i increases.[77] However, previous Ne + SAM simulation results by Hase and co-workers point to a similar dependence of β on E_i, although their incident energies are much smaller.[17] For CO_2 + F-SAM,[6] the values of β decrease monotonically (or almost monotonically) with E_i and this was attributed to the higher frequency of direct events as E_i increases, which are not efficient attaining thermal accommodation. For O_3 + F-SAM the same argument can be employed for low collision energies as direct collisions also increase their frequency as E_i increases. At high E_i, though, penetration is the most likely mechanism for O_3 + F-SAM. Of those trajectories that penetrate inside the monolayer, a fraction of 30−40% spends enough time inside so as to come to thermal equilibrium.

The advantage of the overlap method proposed in this work is that it sorts the trajectories according to whether or not they lead to thermal equilibrium of the gas with the surface. Trajectories that belong to the same collision type may or may not achieve accommodation depending on their residence times. Figure 15 shows the percentage of trajectories that perform single (1ITP) and multiple (nITP) collisions and have residence times greater than $\tau_{res}^{0,acc}$, and therefore lead to accommodation. The analysis is made for both the translational and the rotational degrees of freedom of ozone and for different incident energies. At high incident energies, only multiple collisions contribute to thermal accommodation, as expected. However, at low incident energies, a significant percentage of molecules that perform only one collision with the surface come into thermal equilibrium with the surface. For sufficiently low incident energies, the residence time is long and the molecules start to accommodate their rotational and translational degrees of freedom before the collision. It seems that accommodation is a consequence of gentle changes of the rotational angular momentum or velocity of the center-of-mass of the molecule, rather than the result of a number of abrupt collisions with the surface. This result is in line with our previous NO + F-SAM study where we found, using a more rudimentary analysis, that 86% of the direct events at E_i = 1 kcal/mol contribute to thermal accommodation.[4]

Finally, sometimes the $P(E_f)$ and $P(J)$ distributions can be modeled by two MB components, one at the surface temperature and the other one at a higher temperature T.[6,36] For instance, in our recent CO_2 + F-SAM simulation study the following function

$$P(E_f) = \beta P_{T_S}^{MB}(E_f) + (1 - \beta)P_T^{MB}(E_f) \quad (22)$$

was fit to the trajectory $P(E_f)$ distribution,[6] with T and β being the adjustable parameters. For the present O_3 + F-SAM simulation study, the values of T (the temperature of the high-energy component) can be obtained analytically. In particular, inserting the above result for β (eq 21) into eq 22 and calculating the average of both sides of the equation, T can be expressed as:

$$T = T_S + \frac{a_1 \exp\left(-\frac{b_1}{\sqrt{E_i}}\right) + a_2 \csc h^2\left(\frac{b_2}{\sqrt{E_i}}\right)}{2R(1 - a)\exp(-bE_i)} \quad (23)$$

where T_S = 298 K, a_1, b_1, a_2, and b_2 are the parameters for energy transferred to translation of the scattering ozone (the last column of Table 2), and a and b are the values of Figure 14. Figure 16 shows the dependence of T on the incident energy predicted by eq 23 for O_3 + F-SAM. The previous results for CO_2 + F-SAM, obtained by fitting eq 22 to the trajectory $P(E_f)$ distribution, are also included.[6] Quite remarkably, eq 23 provides temperature values for O_3 + F-SAM that agree reasonably well with the CO_2 + F-SAM temperatures. The strength of eq 23 is that it may be employed to characterize the $P(E_f)$ distributions at any value of E_i without the need of additional experiments or simulations.

dx.doi.org/10.1021/jp309733w | J. Phys. Chem. C 2012, 116, 25454−25464

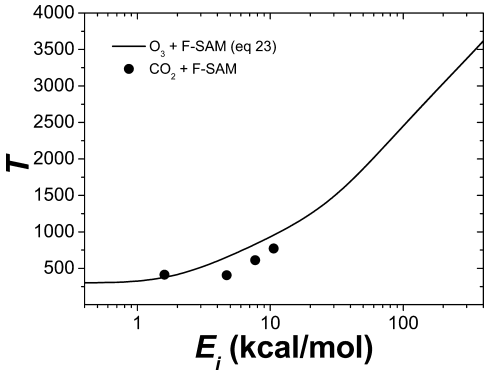

Figure 16. Dependence of the temperature of the high-energy component of the $P(E_f)$ distribution with E_i, obtained for O_3 + F-SAM with eq 23 (solid line) and for CO_2 + F-SAM (circles).[6] The CO_2 + F-SAM results are an average of the temperatures obtained with the explicit-atom and the united-atom models of the F-SAM.

IV. CONCLUSIONS

The O_3 + F-SAM system was studied in this work by chemical dynamics simulations using a potential energy function for the interaction between the projectile and the surface that was developed from a fit to high-level ab initio calculations. The translational distribution of the scattered ozone molecules obtained in our simulations, at an incident energy of 16.75 kcal/mol and incident angle of 30°, agrees reasonably well with the experimental distribution.

A phenomenological model of energy transfer in gas-surface collisions is proposed in this work. The model relies on old energy transfer models for atom−diatom collisions and reproduces very well simulation data over a wide collision energy range for various projectiles colliding with an F-SAM, namely, O_3, NO, and Ar. It predicts energy transfer efficiencies to the surface in the high incident energy limit of close to 100% for atoms and lower for molecules, since the molecules have internal states that share the incident energy with the surface degrees of freedom.

The accommodation coefficients calculated in this work as a function of E_i follow an exponential decay function with decay rates very similar for the translational and rotational degrees of freedom. The accommodation coefficients rather than becoming vanishingly small as E_i increases, they level off around 0.3−0.4. This result indicates that even at very high incident energies, a fraction of molecules come to thermal equilibrium with the surface. A new method to calculate the accommodation coefficients is proposed in this work. The method identifies collision mechanisms with accommodation probabilities. One of the most important results from this analysis is that a significant fraction of direct collisions contribute to accommodation at very low incident energies.

■ ASSOCIATED CONTENT

Supporting Information

New potential parameters for the interaction between NO and the surface employed in this work for the incident energy range 40−500 kcal/mol. This material is available free of charge via the Internet at http://pubs.acs.org.

■ AUTHOR INFORMATION

Corresponding Author

*E-mai: emilio.nunez@usc.es.

Present Address

On leave from Universidad de Extremadura, Spain.

Notes

The authors declare no competing financial interest.

■ ACKNOWLEDGMENTS

M.M.P. acknowledges "Gobierno de Extremadura" and "Fondo Social Europeo" (Project No. IB10001), and J.J.N. acknowledges University of Santiago de Compostela for financial support through their respective PhD fellowships. The authors also thank "Centro de Supercomputación de Galicia (CESGA)" and the LUSITANIA computer at Computaex, Spain, for the use of their facilities.

■ REFERENCES

(1) Cohen, S. R.; Naaman, R.; Sagiv, J. *J. Chem. Phys.* **1988**, *88*, 2757−2763.
(2) Cohen, S. R.; Naaman, R.; Sagiv, J. *Phys. Rev. Lett.* **1987**, *58*, 1208−1211.
(3) Nogueira, J. J.; Sanchez-Coronilla, A.; Marques, J. M. C.; Hase, W. L.; Martinez-Nunez, E.; Vazquez, S. A. *Chem. Phys.* **2012**, *399*, 193−204.
(4) Nogueira, J. J.; Homayoon, Z.; Vazquez, S. A.; Martinez-Nunez, E. *J. Phys. Chem. C* **2011**, *115*, 23817−23830.
(5) Nogueira, J. J.; Vazquez, S. A.; Lourderaj, U.; Hase, W. L.; Martinez-Nunez, E. *J. Phys. Chem. C* **2010**, *114*, 18455−18464.
(6) Nogueira, J. J.; Vazquez, S. A.; Mazyar, O. A.; Hase, W. L.; Perkins, B. G.; Nesbitt, D. J.; Martinez-Nunez, E. *J. Phys. Chem. A* **2009**, *113*, 3850−3865.
(7) Nogueira, J. J.; Martinez-Nunez, E.; Vazquez, S. A. *J. Phys. Chem. C* **2009**, *113*, 3300−3312.
(8) Yang, L.; Mazyar, O. A.; Lourderaj, U.; Wang, J. P.; Rodgers, M. T.; Martinez-Nunez, E.; Addepalli, S. V.; Hase, W. L. *J. Phys. Chem. C* **2008**, *112*, 9377−9386.
(9) Vazquez, S. A.; Morris, J. R.; Rahaman, A.; Mazyar, O. A.; Vayner, G.; Addepalli, S. V.; Hase, W. L.; Martinez-Nunez, E. *J. Phys. Chem. A* **2007**, *111*, 12785−12794.
(10) Martínez-Núñez, E.; Rahaman, A.; Hase, W. L. *J. Phys. Chem. C* **2007**, *111*, 354−364.
(11) Paz, Y.; Naaman, R. *J. Chem. Phys.* **1991**, *94*, 4921−4927.
(12) Day, B. S.; Shuler, S. F.; Ducre, A.; Morris, J. R. *J. Chem. Phys.* **2003**, *119*, 8084−8096.
(13) Gibson, K. D.; Isa, N.; Sibener, S. J. *J. Chem. Phys.* **2003**, *119*, 13083−13095.
(14) Day, B. S.; Morris, J. R. *J. Phys. Chem. B* **2003**, *107*, 7120−7125.
(15) Isa, N.; Gibson, K. D.; Yan, T.; Hase, W.; Sibener, S. J. *J. Chem. Phys.* **2004**, *120*, 2417−2433.
(16) Day, B. S.; Morris, J. R. *J. Chem. Phys.* **2005**, *122*, 234714/1−10.
(17) Yan, T.; Hase, W. L. *Phys. Chem. Chem. Phys.* **2000**, *2*, 901−910.
(18) Yan, T.; Hase, W. L.; Barker, J. R. *Chem. Phys. Lett.* **2000**, *329*, 84−91.
(19) Yan, T.; Hase, W. L. *J. Phys. Chem. A* **2001**, *105*, 2617−2625.
(20) Yan, T.; Hase, W. L. *J. Phys. Chem. B* **2002**, *106*, 8029−8037.
(21) Yan, T.; Isa, N.; Gibson, K. D.; Sibener, S. J.; Hase, W. L. *J. Phys. Chem. A* **2003**, *107*, 10600−10607.
(22) Day, B. S.; Morris, J. R.; Troya, D. *J. Chem. Phys.* **2005**, *122*, 214712/1−12.
(23) Day, B. S.; Morris, J. R.; Alexander, W. A.; Troya, D. *J. Phys. Chem. A* **2006**, *110*, 1319−1326.
(24) Shuler, S. F.; Davis, G. M.; Morris, J. R. *J. Chem. Phys.* **2002**, *116*, 9147−9150.
(25) Ferguson, M. K.; Lohr, J. R.; Day, B. S.; Morris, J. R. *Phys. Rev. Lett.* **2004**, *92*, 073201/1−4.
(26) Li, G.; Bosio, S. B. M.; Hase, W. L. *J. Mol. Struct.* **2000**, *556*, 43−57.
(27) Troya, D.; Schatz, G. C. *J. Chem. Phys.* **2004**, *120*, 7696−7707.

(28) Tasic, U.; Yan, T.; Hase, W. L. *J. Phys. Chem. B* **2006**, *110*, 11863−11877.
(29) Wainhaus, S. B.; Lim, H.; Schultz, D. G.; Hanley, L. *J. Chem. Phys.* **1997**, *106*, 10329−10336.
(30) Schultz, D. G.; Wainhaus, S. B.; Hanley, L.; DeSainteClaire, P.; Hase, W. L. *J. Chem. Phys.* **1997**, *106*, 10337−10348.
(31) Laskin, J.; Futrell, J. H. *J. Chem. Phys.* **2003**, *119*, 3413−3420.
(32) Meroueh, O.; Hase, W. L. *J. Am. Chem. Soc.* **2002**, *124*, 1524−1531.
(33) Troya, D.; Schatz, G. C. *Int. Rev. Phys. Chem.* **2004**, *23*, 341−373.
(34) Alexander, W. A.; Morris, J. R.; Troya, D. *J. Phys. Chem. A* **2009**, *113*, 4155−4167.
(35) Lu, J. W.; Alexander, W. A.; Morris, J. R. *Phys. Chem. Chem. Phys.* **2010**, *12*, 12533−12543.
(36) Perkins, B. G.; Haber, T.; Nesbitt, D. J. *J. Phys. Chem. B* **2005**, *109*, 16396−16405.
(37) Perkins, B. G.; Nesbitt, D. J. *J. Phys. Chem. B* **2006**, *110*, 17126−17137.
(38) Zolot, A. M.; Harper, W. W.; Perkins, B. G.; Dagdigian, P. J.; Nesbitt, D. J. *J. Chem. Phys.* **2006**, *125*, 021101/1−4.
(39) Perkins, B. G.; Nesbitt, D. J. *J. Phys. Chem. A* **2007**, *111*, 7420−7430.
(40) Perkins, B. G.; Nesbitt, D. J. *Proc. Natl. Acad. Sci. U.S.A.* **2008**, *105*, 12684−12689.
(41) Perkins, B. G.; Nesbitt, D. J. *J. Phys. Chem. A* **2008**, *112*, 9324−9335.
(42) Perkins, B. G.; Nesbitt, D. J. *J. Phys. Chem. B* **2008**, *112*, 507−519.
(43) Perkins, B. G.; Nesbitt, D. J. *J. Phys. Chem. A* **2009**, *113*, 4613−4625.
(44) Perkins, B. G.; Nesbitt, D. J. *J. Phys. Chem. A* **2010**, *114*, 1398−1410.
(45) Los, J.; Gleeson, M. A.; Koppers, W. R.; Weeding, T. L.; Kleyn, A. W. *J. Chem. Phys.* **1999**, *111*, 11080−11087.
(46) Koppers, W. R.; Beijersbergen, J. H. M.; Weeding, T. L.; Kistemaker, P. G.; Kleyn, A. W. *J. Chem. Phys.* **1997**, *107*, 10736−10750.
(47) Koppers, W. R.; Gleeson, M. A.; Lourenço, J.; Weeding, T. L.; Los, J.; Kleyn, A. W. *J. Chem. Phys.* **1999**, *110*, 2588−2596.
(48) Wang, J.; Meroueh, S. O.; Wang, Y.; Hase, W. L. *Int. J. Mass. Spectr.* **2003**, *230*, 57−63.
(49) Song, K.; Meroueh, O.; Hase, W. L. *J. Chem. Phys.* **2003**, *118*, 2893−2902.
(50) Levine, R. D. *Molecular Reaction Dynamics*; Cambridge University Press: Cambridge, 2005.
(51) Gibson, K. D.; Isa, N.; Sibener, S. J. *J. Phys. Chem. A* **2006**, *110*, 1469−1477.
(52) Bosio, S. B. M.; Hase, W. L. *J. Chem. Phys.* **1997**, *107*, 9677−9686.
(53) Tasic, U.; Day, B. S.; Yan, T.; Morris, J. R.; Hase, W. L. *J. Phys. Chem. C* **2008**, *112*, 476−490.
(54) Vayner, G.; Alexeev, Y.; Wang, J.; Windus, T. L.; Hase, W. L. *J. Phys. Chem. A* **2006**, *110*, 3174−3178.
(55) Wang, J.; Hase, W. L. *J. Phys. Chem. B* **2005**, *109*, 8320−8324.
(56) Alexander, W. A.; Troya, D. *J. Phys. Chem. A* **2006**, *110*, 10834−10843.
(57) Frisch, M. J.; Trucks, G. W.; Schlegel, H. B.; Scuseria, G. E.; Robb, M. A.; Cheeseman, J. R.; Scalmani, G.; Barone, V.; Mennucci, B.; Petersson, G. A. et al. *Gaussian 09* revision A.02; Gaussian Inc.: Wallingford CT, 2009.
(58) Boys, S. F.; Bernardi, F. *Mol. Phys.* **1970**, *19*, 553−566.
(59) Peterson, K. A.; Woon, D. E.; Dunning, T. H., Jr. *J. Chem. Phys.* **1994**, *100*, 7410−7415.
(60) East, A. L. L.; Allen, W. D. *J. Chem. Phys.* **1993**, *99*, 4638−4650.
(61) Marques, J. M. C.; Prudente, F. V.; Pereira, F. B.; Almeida, M. M.; Maniero, A. M.; Fellows, C. E. *J. Phys. B: At. Mol. Opt. Phys.* **2008**, *41*, 85103−85117.
(62) Tasic, U.; Yan, T.; Hase, W. L. *J. Phys. Chem. B* **2006**, *110*, 11863−11877.
(63) Lu, J. W.; Morris, J. R. *J. Phys. Chem. A* **2011**, *115*, 6194−6201.
(64) Hase, W. L.; Bolton, K.; Sainte Claire, P. d.; Duchovic, R. J.; Hu, X.; Komornicki, A.; Li, G.; Lim, K. F.; Lu, D.-H.; Peslherbe, G. H. et al. *Venus05, a general chemical dynamics computer program*, 2004.
(65) Hu, X.; Hase, W. L.; Pirraglia, T. *J. Comput. Chem.* **1991**, *12*, 1014−1024.
(66) Allen, M. P.; Tildesley, D. J. *Computer Simulation of Liquids*; Clarendon Press: Oxford, 1987.
(67) Alexander, W. A.; Troya, D. *J. Phys. Chem. C* **2011**, *115*, 2273−2283.
(68) Xantheas, S. S.; Atchity, G. J.; Elbert, S. T.; Ruedenberg, K. *J. Chem. Phys.* **1991**, *94*, 8054−8069.
(69) Mahan, B. H. *J. Chem. Phys.* **1970**, *52*, 5221−5225.
(70) Winters, H. F.; Coufal, H.; Rettner, C. T.; Bethune, D. S. *Phys. Rev. B* **1990**, *41*, 6240−6256.
(71) Tasic, U.; Troya, D. *Phys. Chem. Chem. Phys.* **2008**, *10*, 5776−5786.
(72) Gibson, K. D.; Killelea, D. R.; Becker, J. S.; Yuan, H.; Sibener, S. J. *Chem. Phys. Lett.* **2012**, *531*, 18−21.
(73) Miller, S. A.; Luo, H.; Pachuta, S. J.; Cooks, R. G. *Science* **1997**, *275*, 1447−1450.
(74) Knudsen, M. *Ann. Phys.* **1911**, *34*, 593−656.
(75) Goodman, F. O. *J. Phys. Chem.* **1980**, *84*, 1431−1445.
(76) Maxwell, J. C. *Phil. Trans. R. Soc. Lond.* **1879**, *170*, 231−256.
(77) Phillips, L. F.; Nesbitt, D. J. *Chem. Phys. Lett.* **2012**, *546*, 53−57.